Coarsening dynamics of nanodroplets on topographically structured substrates

2013 J. Phys.: Condens. Matter 25 045012

(http://iopscience.iop.org/0953-8984/25/4/045012)

IOP PUBLISHING JOURNAL OF PHYSICS: CONDENSED MATTER
J. Phys.: Condens. Matter **25** (2013) 045012 (13pp) doi:10.1088/0953-8984/25/4/045012

Coarsening dynamics of nanodroplets on topographically structured substrates

M Asgari and A Moosavi

Center of Excellence in Energy Conversion (CEEC), School of Mechanical Engineering, Sharif University of Technology, Azadi Avenue, PO Box 11365-9567 Tehran, Iran

E-mail: moosavi@sharif.edu

Received 17 July 2012, in final form 15 November 2012
Published 4 January 2013
Online at stacks.iop.org/JPhysCM/25/045012

Abstract
Employing a biharmonic boundary integral method with linear elements, coarsening dynamics of nanodroplets on topographical step heterogeneity is investigated. It is shown that the step height and droplet configuration have an influential effect on the dynamics. Increasing the step height slows down the process while locating the droplets close to the step boosts the coarsening rate. Considering a slip boundary condition enhances the dynamics and reveals a transition in the droplet migration direction. Our results reveal that increasing the surface wettability weakens the dynamics. Various types of the disjoining pressure over the step are also considered and their effects on the coarsening are investigated.

(Some figures may appear in colour only in the online journal)

1. Introduction

It is well known that a thin liquid film on a homogeneous solid surface is spinodally unstable if the gradient of the disjoining pressure with respect to the distance from the surface is positive. In this regime, capillary waves are amplified and the film spontaneously breaks up. In an analogy to the spinodal decomposition in the phase separation of binary alloys described by the Cahn–Hilliard equation, this evolution is sometimes called spinodal dewetting [1–4]. However, a spinodally stable thin film could also become unstable in the presence of chemical and physical surface heterogeneities [5–7]. A thin layer of a liquid covering a hydrophobic surface gradually deforms through dewetting mechanisms [8, 9, 5, 10–17], and instabilities lead to the formation of dry spots in the early stages of this process [10, 11]. The resulting holes start to grow and their growth continues until they arrive at neighboring holes. Merging of the neighboring holes causes the liquid layer to evolve into a pattern of ridges, which eventually breaks up into droplets [18–20]. The resultant droplets are not stable yet and continue to change in a slow process called coarsening, whereby droplets drift and exchange mass.

The coarsening is a general phenomenon studied in different contexts, such as phase separation of binary alloys [21–23], and is associated with the decrease in the total number of features (here droplets) and an increase in the average feature size and the average distance between features, and is basically driven by reduction of the total energy of the system. In the context of thin liquid films, this process has recently become the focus of extensive theoretical and numerical investigations which have tried to obtain a general law for the coarsening rate of a large array of droplets. In [24] a reduced model based on asymptotic methods is derived and it is shown that the number of droplets during the coarsening over a homogeneous surface could be evaluated well by $N(t) = O(t^{-2/5})$, where N is the number of droplets and t is time. Obtaining reduced ordinary differential equations has allowed one to consider interactions of large numbers of droplets, which would be time consuming using the underlying partial differential equations. Other studies have shown that considering the effect of physical parameters such as the slip boundary condition and gravity could qualitatively modify the physics. Changing from a no-slip boundary to a slip regime causes the droplets to collide more and alters the coarsening rate [25]. Also, increasing the slip length above a critical value changes the direction of the droplet migration during the coarsening. In the initial stages of this process, droplets are small and with a parabolic profile. However, after sufficient time, gravity will cause the coarsened droplets to flatten into puddles. It is revealed that the coarsening rate for larger droplets decreases in the

presence of gravity while smaller droplets remain mostly unaffected [26]. The influence of gravity leads to a cross-over from power law coarsening to a logarithmic behavior. The coarsening dynamics of nanodroplets has been also probed experimentally and analytically [27–29].

It is shown that the early stages of the dewetting could extensively change in the presence of chemical surface heterogeneities [5, 30–36], physical defects [37], and also both of them [6, 7, 38–40]. The breakup time for thin liquid films on solid surfaces can be substantially smaller if the surface is heterogeneous, either chemically or physically. Although the effect of surface heterogeneities on the early stages of the dewetting has attracted much scientific interest, their effect on the late stage of this process has received little attention. The effects of different chemical substrates, such as stripes, chemical steps and chemical gradients, on the coarsening dynamics were considered in our previous work [41]. It was found that the presence of a chemical heterogeneity can enhance or weaken the coarsening dynamics depending on the pattern type and the position of the droplets on the substrate. Also it was found that increasing the contact angle to values larger than a critical value could change the direction of the droplet migration. In this paper, our purpose is rather to investigate the effect of topographic heterogeneities on the coarsening dynamics. To this end, two nanodroplets are located on this type of heterogeneity and different geometrical and chemical parameters of the topography, such as the step height, the droplet configuration, the step wettability, and the step disjoining pressure, are considered to evaluate their influence on the dynamics.

The paper is organized as follows: first, the governing equations and the numerical method are introduced briefly. Next, the results of the simulations are presented and discussed. The final section of the paper is dedicated to the conclusion.

2. Governing equations and numerical algorithm

In the limit of low Reynolds number, where viscous forces dominate the inertial forces, the Navier–Stokes equations could be simplified to the following equations:

$$\nabla \cdot U = 0, \tag{1}$$

$$\nabla \cdot \gamma = 0, \tag{2}$$

where U represents the velocity vector and $\gamma_{ij} = -P\delta_{ij} + \mu(U_{i,j} + U_{j,i})$ is the stress tensor, where P stands for the pressure, δ_{ij} is the Kronecker symbol and μ denotes the dynamic viscosity of the liquid.

The problem is converted to a non-dimensional form by scaling the lengths by b, which is the equilibrium wetting film thickness, the velocity by Ab/μ, where A is a material-dependent parameter, and the pressure by σ/b, where σ stands for the surface tension. The dimensionless time is given in units of μ/A [42].

By introducing the stream function $\psi(\partial\psi/\partial y = u_x, \partial\psi/\partial x = -u_y)$ and the vorticity $\omega(\omega = \partial u_x/\partial y - \partial u_y/\partial x)$ in terms of the dimensionless velocity $\mathbf{u}(u_x, u_y)$, the governing equations can be reformulated as [43]:

$$\nabla^2\psi = \omega, \tag{3}$$

$$\nabla^2\omega = 0, \tag{4}$$

or equivalently, from the above set of equations, one can show that $\nabla^4\psi = 0$.

Suitable boundary conditions for this system are discussed in detail by [41]. Employing the fluid–vapor interface boundary conditions yields the following:

$$\omega = 2\psi_{ss} - 2\kappa\psi_n, \tag{5}$$

$$\omega_n = -2\psi_{nss} + 2\kappa\psi_{ss} + 2\kappa_s\psi_{ss} - \frac{\kappa_s + \Pi}{\tilde{C}}, \tag{6}$$

where s is the arc length derivative and κ stands for the curvature and may be calculated from:

$$\kappa = \frac{y_{ss}x_s - x_{ss}y_s}{(x_s^2 + y_s^2)^{3/2}}. \tag{7}$$

The parameter $\tilde{C}$ is a scaling factor and the time is scaled by $\mu b/(\tilde{C}\sigma)$ [42]. The value of this parameter in this study is taken to be 3 for all the cases to simplify the comparisons.

The presence of the intermolecular interactions could be summarized into Π, which is the disjoining pressure (DJP). The DJP is defined as the derivative of the intermolecular potential energy V:

$$\Pi = -\frac{\mathrm{d}V}{\mathrm{d}y}. \tag{8}$$

On homogeneous flat substrates V is independent of the lateral dimension, but for physical (or chemical) heterogeneous surfaces V changes laterally. In most of the previous studies lateral variation of the disjoining pressure has been modeled crudely. In the other words, a heterogeneous substrate is assumed to be locally homogeneous and lateral interferences of heterogeneities are neglected [44, 45, 36, 46, 47]. Recently, a more refined representation of the heterogeneity was introduced [42]. In this model the pairwise interactions of the particles are modeled as $U_{\alpha\beta}(r) = \frac{M_{\alpha\beta}}{r^{12}} - \frac{N_{\alpha\beta}}{r^6}$, where α and β relate to liquid (l), substrate (s) or coating particles (c), $M_{\alpha\beta}$ and $N_{\alpha\beta}$ are material parameters and r is the interatomic distance. Then the general formulation of the disjoining pressure could be given by:

$$\Pi(r) = \int_{V_s} \{\rho_l^2\, U_{ll}(r - r') - \rho_l\, \rho_s\, U_{sl}(r - r')\}\, \mathrm{d}r^3, \tag{9}$$

with $r, r' \in \Re^3$ and ρ_l, ρ_s as the number densities of the liquid and substrate, respectively. V_s is the substrate volume. For a homogeneous substrate, this formulation results in a DJP with the following form:

$$\Pi_h(y) = C\left(\frac{1}{y^9} \mp \frac{1}{y^3} + \frac{B}{y^4}\right). \tag{10}$$

The parameter C is a dimensionless amplitude which compares the strength of the effective intermolecular and the surface tension forces. C is called the capillary number and

Table 1. The different terms in the disjoining pressure of step topography.

Term	Formulation
I_e^{12}	$\frac{\Pi}{11\,520x^9y^9(x^2+y^2)^{\frac{7}{2}}}[-280x^6y^6(x^4+y^4)-448x^2y^2(x^{12}+y^{12})-128(x^{16}+y^{16})+128(x^9+y^9)(x^2+y^2)^{\frac{7}{2}}-35x^8y^8-560x^4y^4(x^8+y^8)]$
I_e^{6}	$\frac{\Pi}{24x^3y^3\sqrt{x^2+y^2}}[2(x^3+y^3)\sqrt{x^2+y^2}-2(x^4+y^4)-y^2x^2]$
I_c^{12}	$\frac{\Pi d}{1280(x^2+y^2)^{\frac{9}{2}}y^{10}}[128(x^2+y^2)^{\frac{9}{2}}-315xy^8-840x^3y^6-1008x^5y^4-576x^7y^2-128x^9]$
I_c^{6}	$\frac{\Pi d}{8y^4(x^2+y^2)^{\frac{3}{2}}}[-2(x^2+y^2)^{\frac{3}{2}}+3xy^2+2x^3]$

defined as $C = Ab/\sigma$. The parameter B controls the shape of the DJP. Depending on the sign of the long-range term (minus or plus) in equation (10), the system can exhibit different dynamics [42]. These cases have been referred to as the minus and the plus cases [42], respectively. The equilibrium contact angle at any location is defined as the following:

$$\cos\theta_{\mathrm{eq}} = 1 + \int_{y_0}^{\infty} \Pi(y)\,\mathrm{d}y, \tag{11}$$

where y_0 stands for the precursor film thickness ($\Pi(y_0) = 0$) [42]. This simple DJP is just a function of the normal coordinate. A more realistic model can be built by superposing the effect of all the flat substrates such that for the droplet positioned on the top side of the step, the effect of horizontal plate below it is considered, but for the droplet on the bottom side of the step, the DPJ includes the effect of vertical plate and the horizontal plate below the droplet, i.e.,

$$\begin{aligned}
&\Pi_{\mathrm{step}}(x<0, y) = \Pi_h(y-h),\\
&\Pi_{\mathrm{step}}(x>0, y<h) = \Pi_h(x) + \Pi_h(y),\\
&\Pi_{\mathrm{step}}(x>0, y>h) = \Pi_h(y).
\end{aligned} \tag{12}$$

h represents the height of the step.

A substantial improvement on modeling of the DJP over the step can be obtained by decomposing the step into contributions from quarter spaces (edges) forming building blocks which can be calculated analytically by solving the integral of equation (9). Here, we mention a brief description of the model formulation, while details of the explanations are presented in [42]. The disjoining pressure of the left upper edge is:

$$\Pi^l(x,y) = \Pi_e^l(x+d, y+d) + \Pi_c^{l-h}(x,y) + \Pi_c^{l-v}(x,y), \tag{13}$$

where d is the coating layer thickness, Π_e represents the effect of the edge, Π_c is the effect of the coating layer and the superscripts h and v stand for the horizontal and vertical layers, respectively. The DJP of the edge and the coating layer are defined as:

$$\begin{aligned}
\Pi_e^l &= \Delta M_s I_e^{12} - \Delta N_s I_e^6,\\
\Pi_c^{l-h} &= \Delta M_c I_c^{12} - \Delta N_c I_c^6,\\
\Pi_c^{l-v}(x,y) &= \Pi_c^{l-h}(y,x),
\end{aligned} \tag{14}$$

where $\Delta M_x = \rho_l^2 M_{ll} - \rho_l\rho_x M_{lx}$ and $\Delta N_x = \rho_l^2 N_{ll} - \rho_l\rho_x N_{lx}$. The different terms in equation (14) are given in table 1.

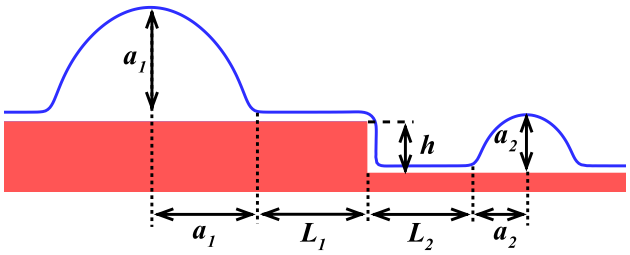

Figure 1. Two droplets are placed on a topographic step. L_1 and L_2 determine the droplet distances from the step while a_1 and a_2 indicate their radii. h is the step height.

Using the definition of the left edge DJP and symmetry of the system, the total disjoining pressure is obtained as:

$$\Pi(x,y) = \Pi^l(x, y-h) + \Pi^l(-x, y) - 2\Pi_c^{l-v}(x,y). \tag{15}$$

The last term on the right-hand side of equation (15) removes the effect of the artificial extra coatings on the left and the right quarter spaces (at $x = 0, y < 0$) which get buried upon building the step out of the coated edges.

In order to study the dynamics, we obtain the evolution of mass and position of the droplets during the process. As the simulation is two dimensional, the surface area of the droplets with the assumption of constant density is used to measure their mass. The position of the droplets is determined by obtaining their center of mass in the lateral direction (x axis). Equations (16) and (17) define the surface area (mass) and center of mass of the droplets, respectively.

$$M_i = \int_{S_i} \mathrm{d}A, \tag{16}$$

$$X_i = \frac{\int_{S_i} X\,\mathrm{d}A}{\int_{S_i}\mathrm{d}A}, \tag{17}$$

where M_i/X_i represents the mass/position of smaller ($i = s$) or larger ($i = l$) droplets and S_i is the surface area occupied by each droplet.

3. Results

To investigate the coarsening dynamics of two nanodroplets located on the step topography, it is assumed that the system has an initial condition illustrated in figure 1. The different parameters shown in this figure are the focus of this section to study how they affect the dynamics. The larger and the

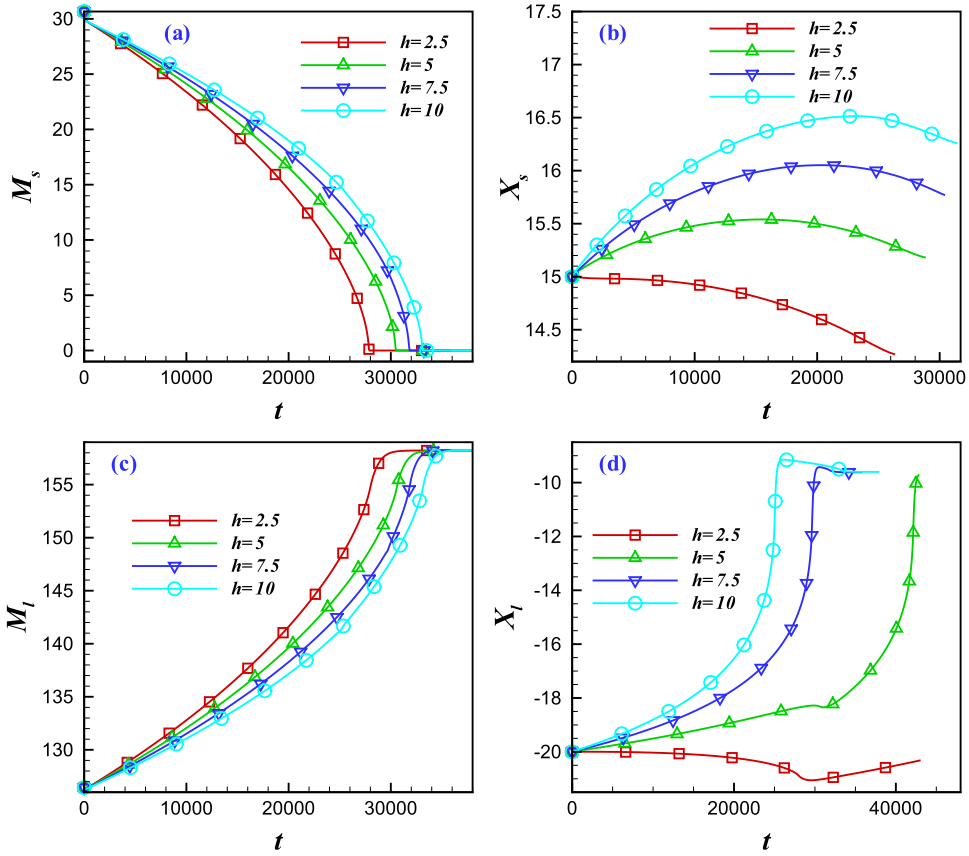

Figure 2. Effect of the step height on the coarsening dynamics. The collapse of the smaller droplet (a), migration of the smaller droplet (b), growth of the larger droplet (c), and migration of the larger droplet (d) are compared for various step heights. The radius and height of the larger droplet are twice those of the smaller one, with values of 10 and 5, respectively. The minus DJP is considered with a (B, C) equal to $(0, 3)$. (L_1, L_2) are both supposed to be 10.

smaller droplets are positioned at distances L_1 and L_2 from the step and their initial radii are a_1 and a_2, respectively. The step height is indicated by h. To start with a reasonably close profile to the relaxed droplet profile, we consider a parabola profile that is centered about $x = \bar{x}$ and is smoothly connected to the ultra-thin film (UTF), that is:

$$y(x, t = 0) = y_0 + a\left[1 - \left(\frac{|x - \bar{x}|}{a}\right)^2\right]^{|x-\bar{x}|^m+1}, \quad (18)$$

with the droplet height a in the center being equal to half the base width. y_0 represents the film thickness ($\Pi(y_0) = 0$). Considering an equal initial height and radius facilitates droplets to reach the equilibrium [48]. In this study, we choose m, which determines the smoothness of the transition region from the droplet to the UTF, to be 10.

3.1. Step height

In order to study the influence of the step height on the coarsening dynamics, a series of simulations was conducted for different values of h. Other parameters were kept fixed to remove their influence on the dynamics. Changing the step height alters the distribution of the disjoining pressure over the step and modifies the droplet motion near the step [42].

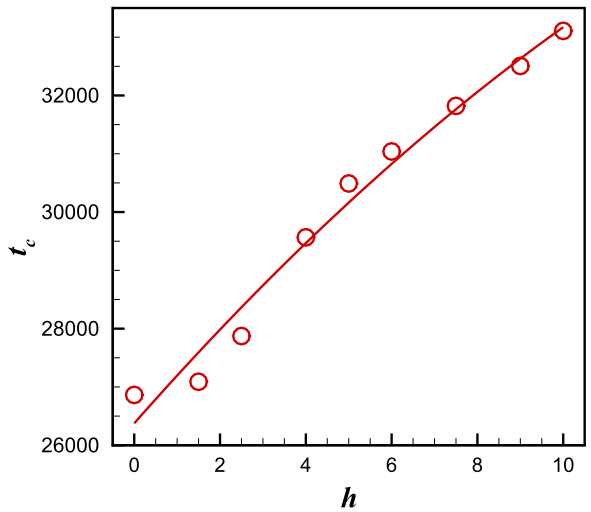

Figure 3. The collapse time of the droplet as a function of the step height. Increasing the step height increases the distance between the droplets and, consequently, increases the collapse time. It is obvious that the slope reduces with h. This is due to the DJP effect and the droplet migration.

On the other hand, changing h is equivalent to changing the distance of the droplets, which plays an important role in the coarsening dynamics, as shown in [41]. The initial

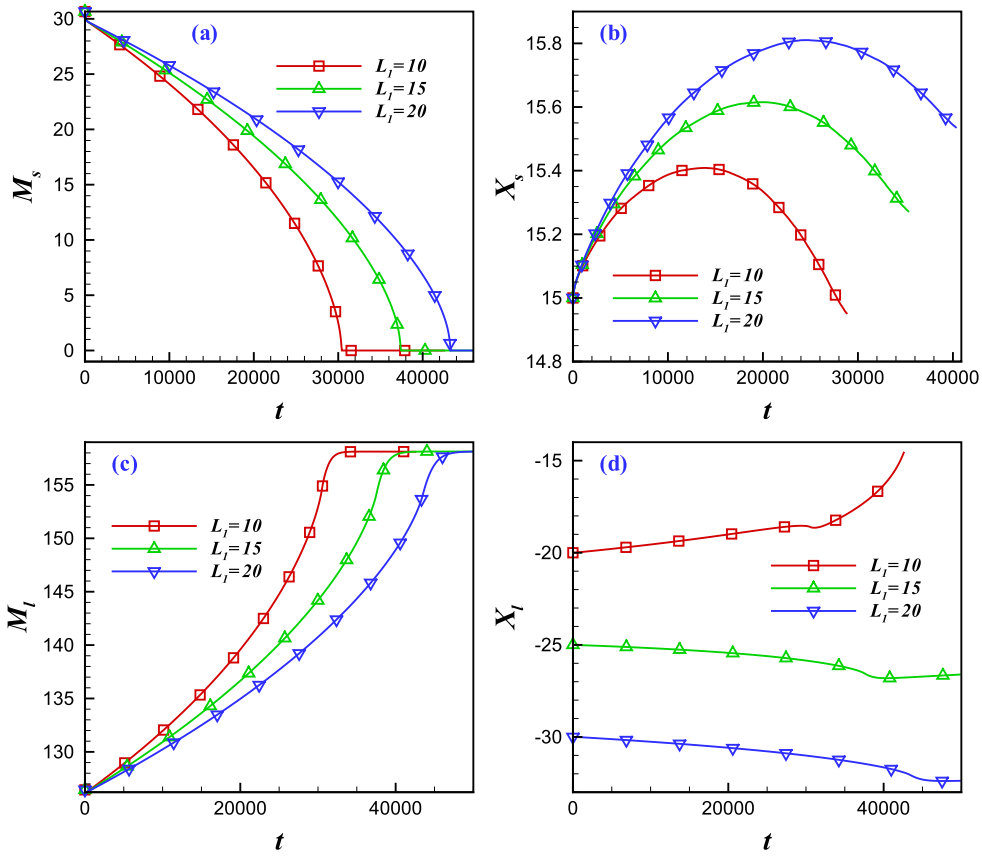

Figure 4. Effect of L_1 (larger droplet distance from the step) on the coarsening dynamics. The radius and height of the larger droplet are twice those of the smaller one, with values of 10 and 5, respectively. The results are for the minus DJP with the (B, C) equal to (0, 3). The step height is 5 and the smaller droplet is positioned at a distance 10 from the step ($L_2 = 10$).

radii of the larger and the smaller droplets are chosen such that the radii ratio is equal to 2, consistent with the work of [49], with values of 10 and 5, respectively. The simulations were conducted for the minus case of the DJP with the parameters (B, C) equal to (0, 3). As already explained, C is the capillary number, which indicates the surface wettability and the contact angle. The initial distances of the droplets from the step (L_1, L_2) are both 10. Results are depicted in figure 2, which includes the evolution of mass and position of the droplets. M_s and M_l represent the surface areas of the smaller and the larger droplets, respectively, which are proportional to the mass with the assumption of constant density. X_s and X_l are the centers of mass of the droplets in the horizontal direction. By increasing the step height, the coarsening rate slows down. This can be associated with the increase of the droplet distance due to the increase of the step height. It is also clear that the growth of the coarsening time reduces on increasing h. The disjoining pressure is enhanced by increasing h and this alters the direction of the migration of the droplets, as shown in figures 2(b) and (d). The time required for complete disappearance of the smaller droplet could be termed as the collapse time. The collapse time could be defined numerically as the time in which the amount of calculated mass for the smaller droplet becomes lower than a specified value (e.g. 0.005). Figure 3 depicts the collapse time of the smaller droplet for various step heights. For a small step height, droplets move in the opposite direction of the x-axis due to the coarsening process, similar to the cases with a homogeneous surface [41]. Increasing the step height intensifies the disjoining pressure and drives the droplets in the positive direction of the x-axis [42]. This decreases the distance between the droplets and enhances the coarsening. Thus, the slope of the coarsening time as a function of the step height reduces.

3.2. Initial position of the droplets

The initial distances of the droplets from the step, (L_1, L_2) shown in figure 1, play an important role in the coarsening dynamics by determining the distance of the droplets and the influence of the DJP on the droplets. To find the effect of these parameters, simulations were performed for different configurations of the droplets. To this end, the initial radii of the droplets are chosen as $a_1 = 10$ and $a_2 = 5$, in analogy to the previous section. The minus case of the disjoining pressure is considered with (B, C) equal to (0, 3) and the step height was kept constant $h = 5$ for all the cases. Figure 4 represents the results for the mass and position of the droplets for $L_2 = 10$ and various values of L_1. As expected, the collapse process slows down on increasing L_1. This can be explained by noting the fact that increasing L_1 increases the distance between the droplets. To quantify the amount of the coarsening time

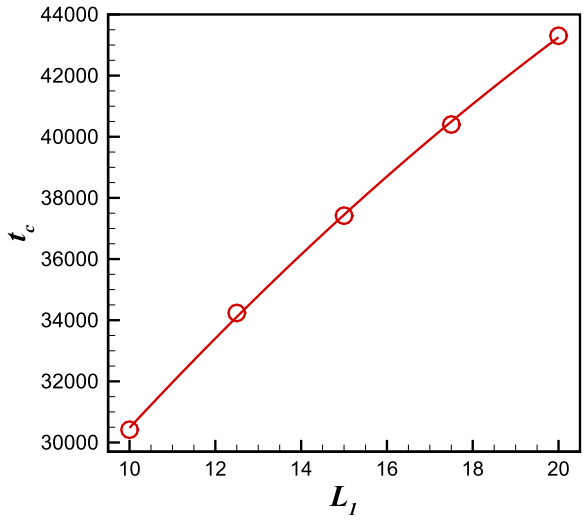

Figure 5. The coarsening time versus the distance of the larger droplet from the step. Increasing L_1 results in the droplet distance increasing and also increases the collapse time. Reduction of the rate could be explained by considering droplet migration due to the DJP.

increase due to L_1 growth, figure 5 illustrates the time as a function of the distance. Changing the distance from 10 to 15 increases the coarsening time more than the case with changing the distance from 15 to 20. Since this behavior is not seen in the case of a homogeneous substrate, where the collapse time increases linearly with the distance [41], the reason can only be explained in terms of the step disjoining pressure. In the vicinity of the step, the minus disjoining pressure drives the droplet on the top side toward the step (in the positive direction of the horizontal axis) [42], which is seen for the smallest distance ($L_1 = 10$) in figure 4. Movement of the larger droplet toward the step reduces the distance of the droplets and enhances the dynamics. When a droplet is positioned far from the step, similar to the cases ($L_1 = 15, 20$), the effect of the DJP on it decreases and the droplet moves in the negative direction of the horizontal axis due to the coarsening such that the distance between the droplets increases. This transition in the direction of the larger droplet movement is clear in figure 4. Therefore, it is expected that increasing L_1 has a noticeable influence when this transition occurs ($10 < L_1 < 15$ in this case).

In order to discuss the effect of L_2, namely, the distance of the smaller droplet from the step, a series of simulations were performed for various values of L_2. In all the simulations the larger droplet distance from the step was kept fixed equal to 10. Figure 6 depicts the different properties of the system as a function of the time. Again it is observable that increasing L_2 slows down the coarsening because the distance between

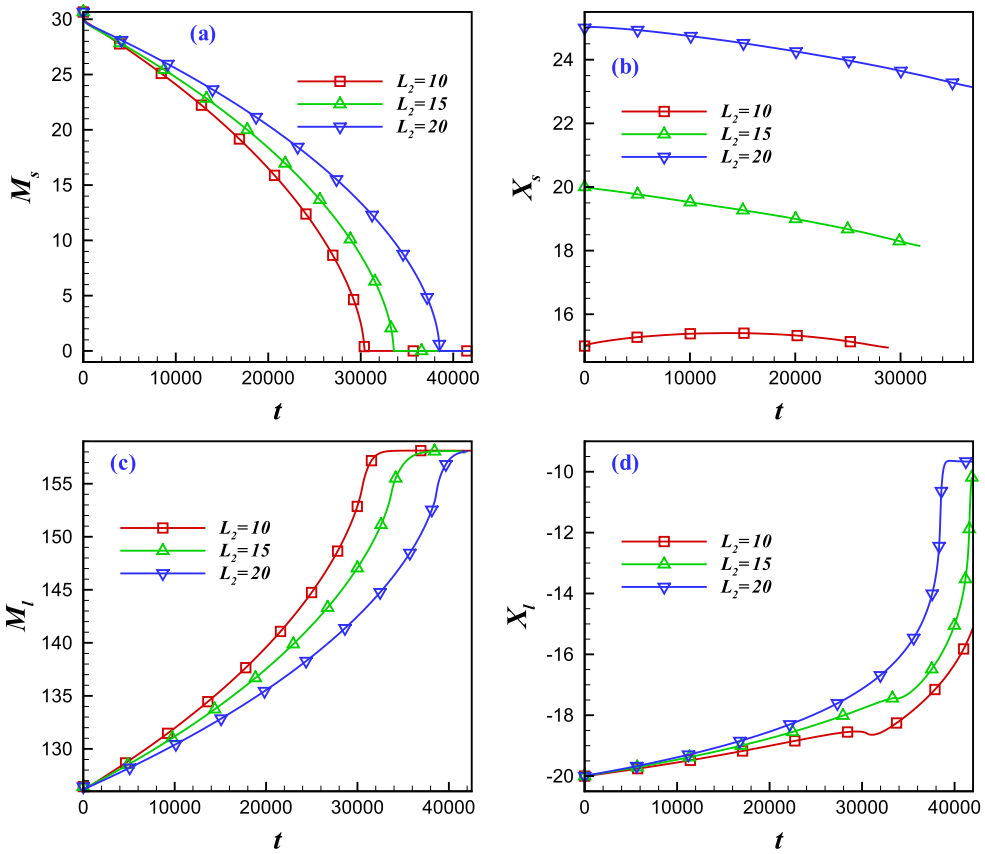

Figure 6. Effect of L_2 (smaller droplet distance from the step) on the coarsening dynamics. The radius and height of the larger droplet are twice those of the smaller one, with values of 10 and 5, respectively. The considered DJP is the minus case with (B, C) equal to (0, 3). The step height is 5 and the larger droplet is positioned at a distance equal to 10 from the step ($L_1 = 10$).

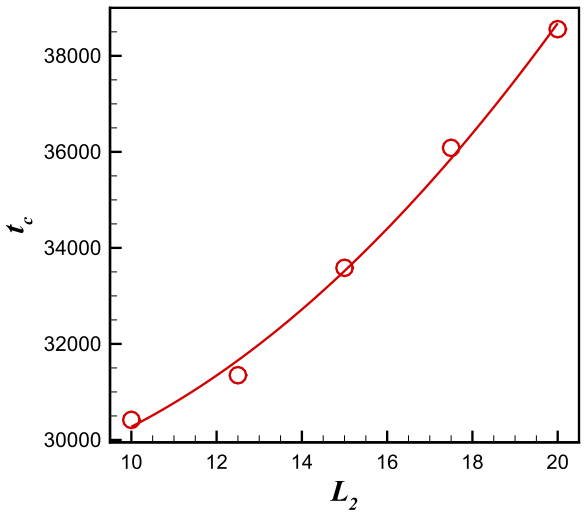

Figure 7. The coarsening time versus the distance of the smaller droplet from the step. Increasing L_2 results in an increase in droplet distance and increases the collapse time. The increase of the rate could be explained by considering the droplet migration due to the DJP.

the droplets increases. Figure 7 shows how the collapse time changes by increasing L_2. This figure proves the time increase due to the distance L_2 growth. Another remarkable point is that increasing the distance from 15 to 20 increases the coarsening time more than the case with increasing the distance from 10 to 15. This behavior can be explained similarly to the L_1 case. In the vicinity of the step, the negative disjoining pressure of the topography causes the lower droplet (here the smaller droplet, refer to figure 1) to leave the step and move in the positive direction of the horizontal axis in our case [42]. This kind of movement is clear in figure 6 just for the smallest distance ($L_2 = 10$). Moving away from the step makes the distance between the droplets larger and decelerates the coarsening. When the droplet is located far from the step ($L_2 = 15, 20$), the effect of the disjoining pressure reduces and the droplet moves in the opposite direction due to the coarsening. This effect of the DJP makes the collapse time difference smaller between the first two cases ($L_2 = 10$ and $L_2 = 15$) and explains the nonlinearity of the coarsening time as a function of the distance.

3.3. Displacing the droplet position

It is desirable to know how the dynamics would change if the positions of the droplets are displaced. In all the former sections, it was assumed that the larger droplet was placed on the top side and the smaller one on the bottom side of the step, as depicted in figure 1. Here, the configuration of the droplets is modified as shown in figure 8. Similar to section 3.1, the height of the step in the new configuration was changed and simulations were conducted. Again, the initial radii of the droplets are 10 and 5, respectively, and their initial distances relative to the step are both 10. The negative disjoining pressure is considered with $B = 0$ and $C = 3$. Various parameters of the system, including the masses

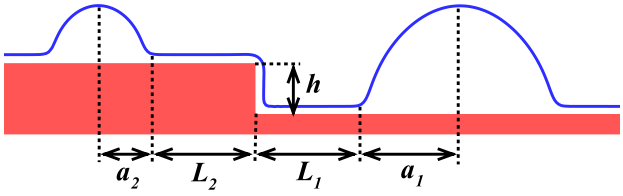

Figure 8. Displacing the droplets such that the smaller and the larger droplets are positioned on the top and bottom sides of the step, respectively. L_1 and L_2 stand for the droplet distances from the step while a_1 and a_2 indicate their radii. h represents the step height.

and positions of the droplets, are illustrated in figure 9. An increase of the collapse time is evident when the height of the step becomes larger, which was also seen in section 3.1 for the reverse structure, but there is no longer a transition in the droplet migration direction. In this new droplet structure, coarsening leads to a movement in the positive direction of the horizontal axis, which is in the same direction as the disjoining pressure force. Therefore, both types of migration (due to coarsening and disjoining pressure) enhance each other and there is no transition in the movement of the droplets. Figure 10 depicts how the coarsening time changes due to the step height increase in the new configuration. It is apparent that the rate increases when h is increasing. This could be related to the disjoining pressure effect, which increases the distance of the droplets and slows down the coarsening. Thus, an increase of h, which intensifies the disjoining pressure, could decelerate the process.

3.4. Slip boundary condition

The effect of considering the slip boundary condition with different slip lengths on the coarsening dynamics has been previously explored in the case of homogeneous [25] and chemically structured surfaces [41]. In order to explore the effect of the slip on topographic structures, two droplets with initial radii of 10 and 5 are considered on a topographic step with height of $h = 5$. The initial distances between the droplets and the step are ($L_1, L_2 = 10$) and the problem is studied for the minus DJP with (B, C) equal to $(0, 3)$. The results are obtained for a range of slip lengths to show the effect of this parameter on the mass evolution and the migration of the droplets (see figure 11). Increasing the slip length enhances the dynamics and reduces the collapse time of the smaller droplet, which is consistent with the results of [25, 41]. Figure 12 illustrates how the total time of coarsening changes due to the slip parameter. When the regime is changed from the no-slip boundary condition ($\beta = 0$) [41] to the slip boundary condition ($\beta > 0$), a transition occurs in the droplet migration direction, as shown in figure 11. From the transition it could be concluded that coarsening dominates when we have a slip regime. In other words, droplets move in the direction of the disjoining pressure force for the no-slip regime, but they move in the direction of the mass flux when there is slippage. The speed of migration of both droplets grows due to the slip length increase.

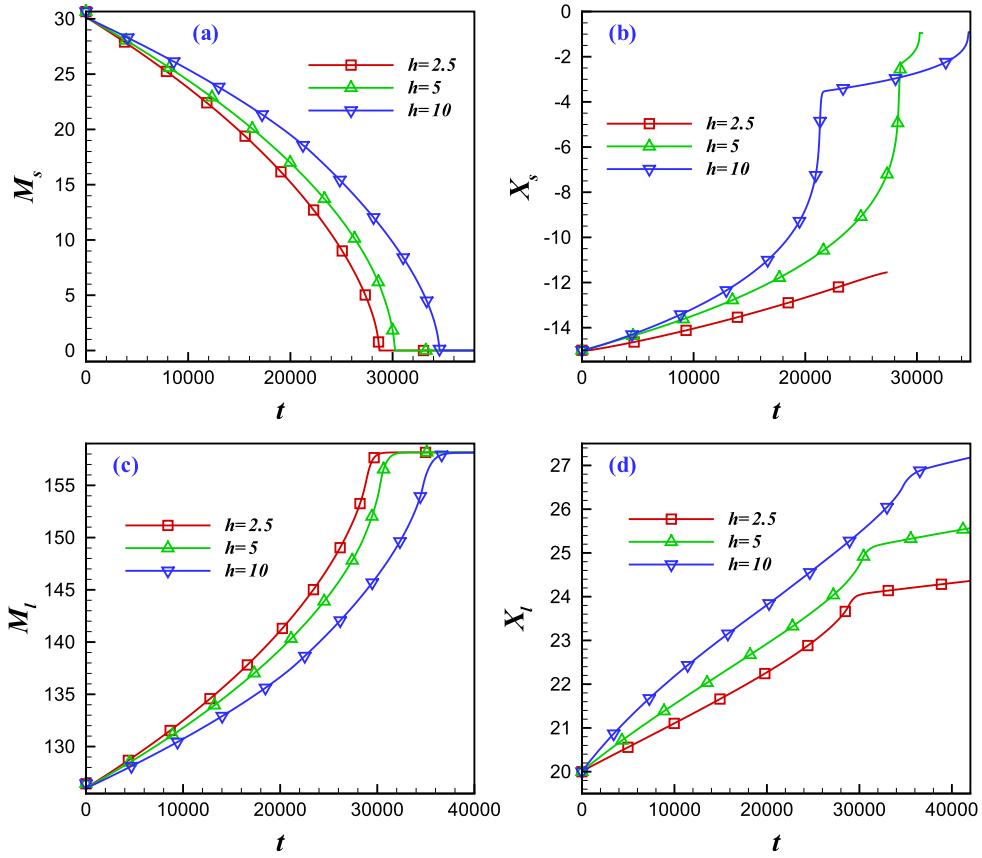

Figure 9. Effect of the step height on the coarsening dynamics when the droplets are displaced and positioned in the new configuration. The radius and height of the larger droplet are twice those of the smaller one, with values of 10 and 5, respectively. The results belong to the minus DJP with (B, C) equal to (0, 3). (L_1, L_2) are both 10.

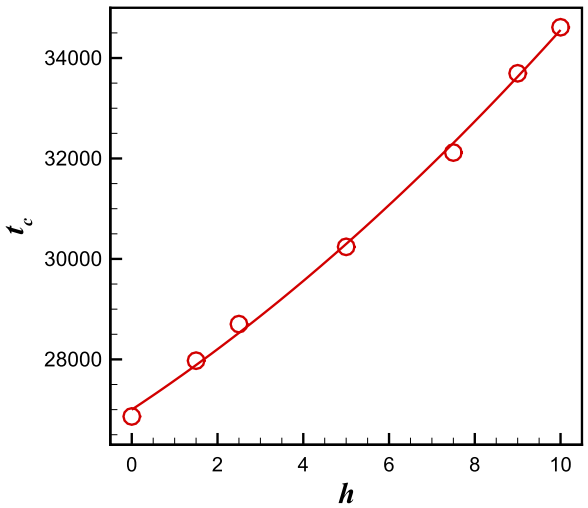

Figure 10. The collapse time versus the step height for the new configuration. Increasing the step height increases the distance between the droplets and, consequently, increases the collapse time. It is obvious that the slope increases by h, which is due to the DJP effect and the droplet migration.

3.5. Surface wettability and the disjoining pressure

In previous sections, our attention was concentrated on the effect of the step height and the initial positions of the droplets on the dynamics. The effects of chemical properties of the substrate and the type of the disjoining pressure were neglected. However, it is reported that the surface wettability and the type of the disjoining pressure could affect the droplet migration and pressure, and thus change the dynamics [42]. To evaluate the effect of these parameters, other properties of the system are fixed. The initial radii of the larger and smaller droplets are (10, 5) respectively. The step height is considered to be 5 and the initial distances between the droplets and the step are (L_1 and $L_2 = 10$). First, results are presented for different surface contact angles for the minus case of the disjoining pressure with ($B = 0$). Figure 13 illustrates how the dynamics is prone to change due to the surface wettability. By increasing the contact angle (reducing wettability of the surface) the collapse time reduces, as is clear in figure 13(a). This is consistent with the results of droplet coarsening on a homogeneous surface [41]. It is worth mentioning that all the cases simulated for this part have large surface contact angles ($\theta_{eq} \geq 90$) and it is not expected to see a transition in the direction of droplet movement as reported for homogeneous surfaces [41]. Here, another kind of transition is clear in the droplet motion when the contact angle is increased, which is due to the step topography disjoining pressure (see figure 13). In other words, competition between coarsening and the disjoining pressure determines the direction of the droplet migration. For smaller contact angles, such as ($\theta_{eq} = 90$),

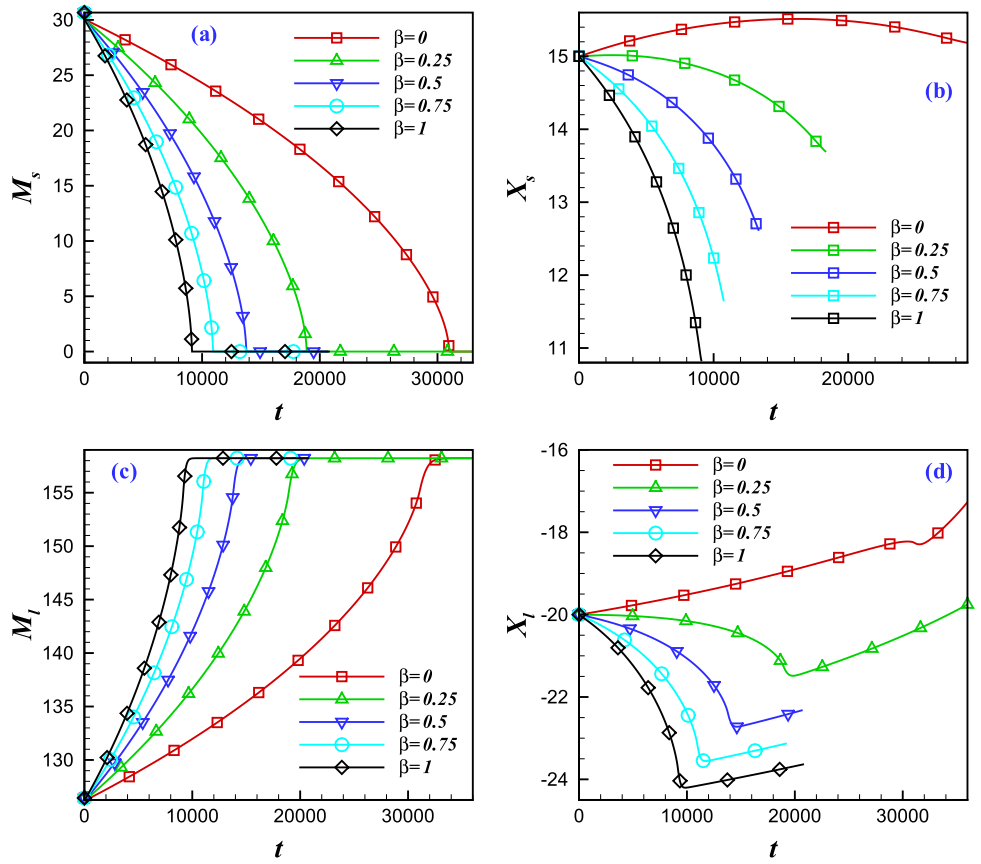

Figure 11. Effect of the slip length on the coarsening dynamics. The radius and the height of the larger droplet are twice those of the smaller one, with values of 10 and 5, respectively. The results are for the minus DJP with (B, C) equal to (0, 3). The height of the step is equal to 5 and (L_1, L_2) are both 10.

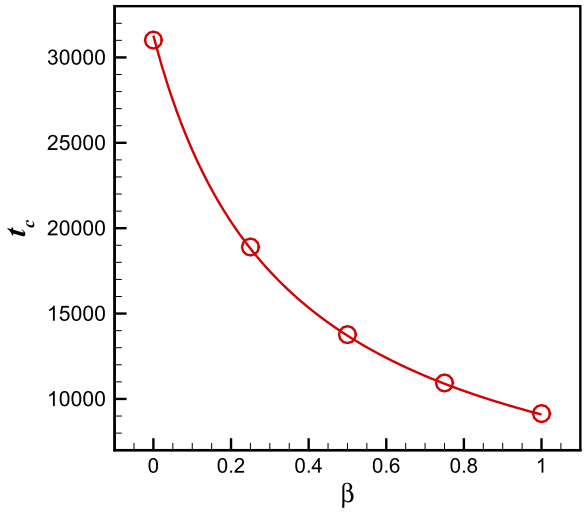

Figure 12. The collapse time versus the slip length when the droplets are positioned on the step topography. The required time reduces when the size of the slip length is increased. This behavior also was previously observed in the case of homogeneous and chemically heterogeneous surfaces [25, 41].

the winner of this competition is the disjoining pressure, which leads the droplets to move in a positive direction of the x-axis. By increasing the contact angle, droplets migrate in the opposite direction (the negative direction of the x-axis), which is due to the coarsening dynamics.

As discussed in introduction, the disjoining pressure can be in the minus and the plus forms. The disjoining pressure is specified using a pair of parameters (B, C). The type of the DJP and the values of (B, C) have been shown to affect the droplet motion near the step [42]. Here, the purpose is to find out if the type of DJP and the values of (B, C) could modify the coarsening dynamics. Also the results of an approximate model of the DJP (obtained from equation (12)) for the coarsening process are examined. Contours of the minus and the plus step DJP are shown for different assumed interface locations in figure 14. This figure is just provided to illustrate how the disjoining pressure could vary along the coordinate system.

First, the minus DJP with different (B, C) but the same contact angle ($\theta_{eq} = 90$) is considered and the results are illustrated in figure 15. The values of (B, C) are (1, 7.7583) with $y_0 = 1.3$, (0, 2.6667) with $y_0 = 1$, and (-1, 1.2703) with $y_0 = 0.88$. For the case ($B = 0, C = 2.6667$), the refined model of the disjoining pressure (equation (14)) is compared with the approximate one (equation (12)).

The effect of the disjoining pressure is intensified when B is increased, as is apparent in figures 15(b) and (d), where the droplets move faster in the direction of the DJP force with increasing B. This is in agreement with the results of [42].

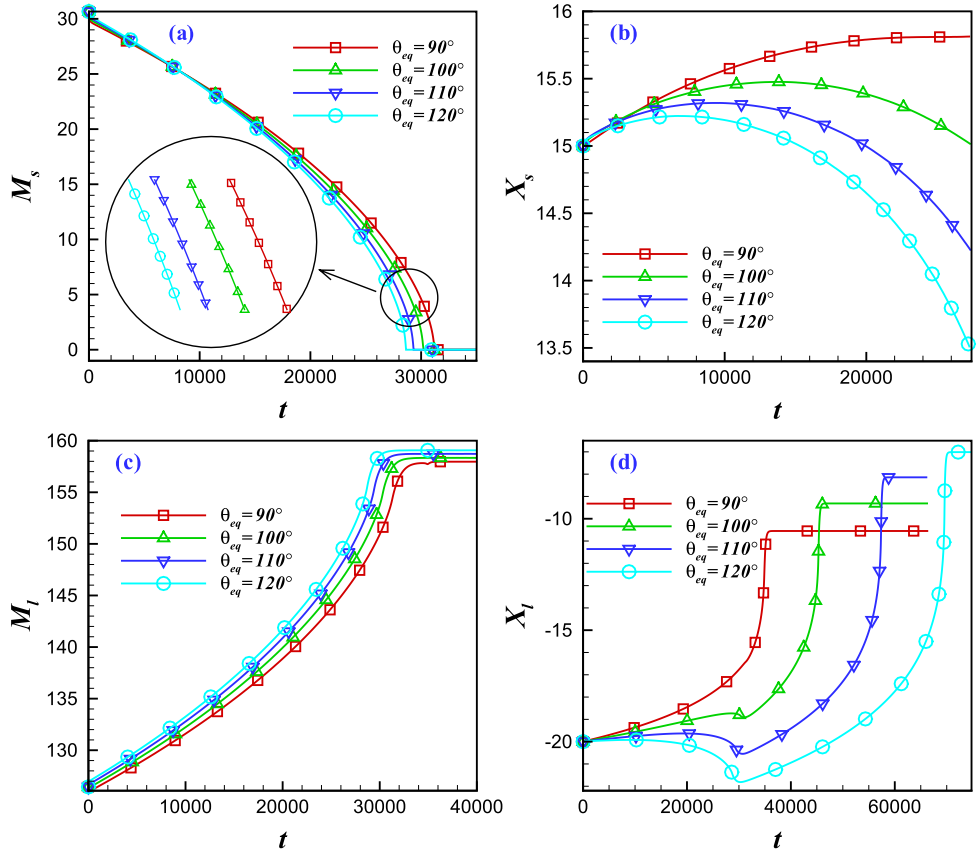

Figure 13. Effect of the surface contact angle on the coarsening dynamics. The radius and height of the larger droplet are twice those of the smaller one, with values of 10 and 5, respectively. The results are for the minus DJP with $B = 0$. The step height is equal to 5 and both the droplets are positioned at a distance 10 from the step ($L_1, L_2 = 10$).

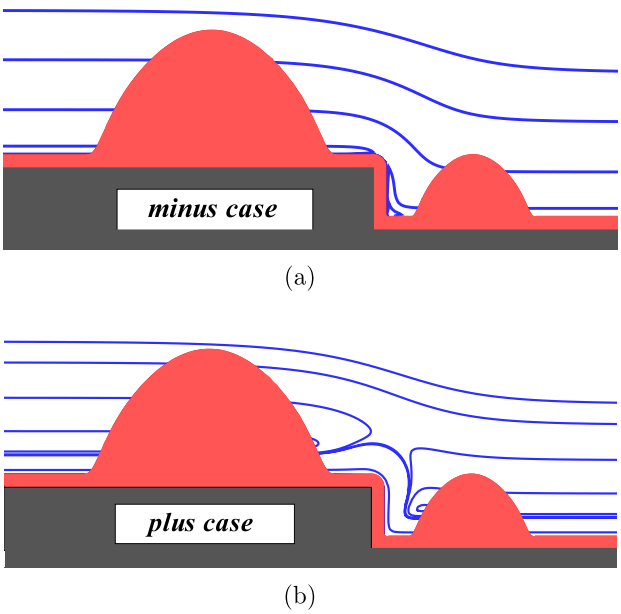

Figure 14. Contours of the step disjoining pressure. (a) The minus DJP with $B = 0$ and (b) the plus DJP with $B = -2.5$. In this figure the values of the disjoining pressure are illustrated for different assumed interface locations to show how it could vary along the coordinate system.

This accelerates the coarsening because the droplets approach each other. Also it should be noted that increasing B leads to a larger film thickness, which could play an important role in accelerating coarsening dynamics. It is shown that for the same pressure gradients the flow rate through the film is proportional to the cube of the film thickness $y_f \approx y_0$, i.e., $Q \propto y_f^3$ [50]. This may explain why for the cases with larger film thickness coarsening occurs faster. The approximate model of the disjoining pressure results in a similar mass evolution for both the droplets in comparison with the more refined model of the DJP. However, there is a noticeable change in the droplet migration when the approximate model is used. This could be related to the fact that the approximate model does not have any influence on the droplet on the top side (here the larger droplet) in the lateral direction, while it exerts an intense force on the droplet on the base part (here the smaller one).

By employing the plus form of the disjoining pressure, coarsening is investigated for two sets of (B, C) values. The chosen values of (B, C) are (-2.5, 4.2327) with $y_0 = 0.91$ and (-4, 0.9265) with $y_0 = 0.79$. Both the cases result in a contact angle equal to 90°. The results are almost the same as the minus DJP, as illustrated in figure 16 in which the collapse time is reduced when the value of B is increased ($-4 \rightarrow -2.5$). This behavior could be related to the film thickness growth and the effect of the disjoining pressure on

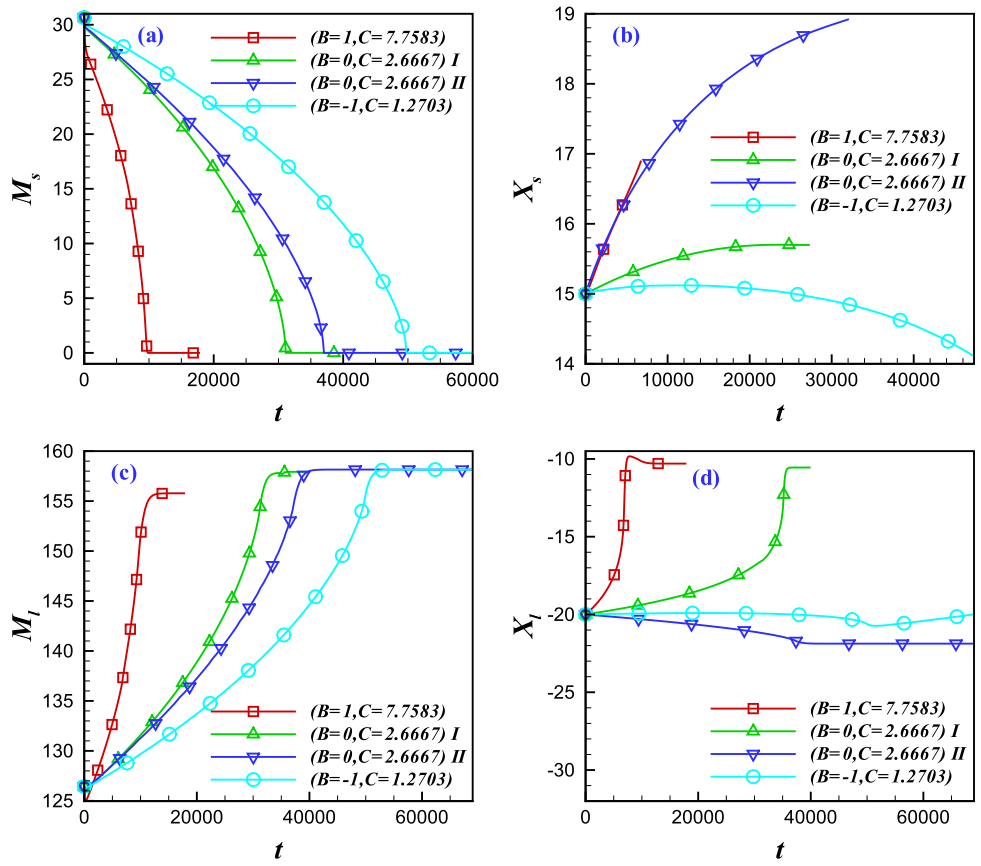

Figure 15. The effect of (B, C) on the coarsening dynamics. The results are for the minus case of the DJP and B and C are selected such that $\theta_{eq} = 90°$. For the case $(B = 0, C = 2.6667)$, the refined model of the disjoining pressure (specified in the legend by *I*) is compared with the approximate one (specified in the legend by *II*). The radius and height of the larger droplet are twice those of the smaller, with values of 10 and 5, respectively. The step height is 5 and both the droplets are positioned at a distance 10 from the step $(L_1, L_2 = 10)$.

the droplets migration, which bring the droplets nearer each other, similar to the minus case (see figure 16). A new feature of the dynamics, in comparison with the minus DJP, is the change of the direction of droplet migration, which is due to the disjoining pressure effect near the step [42]. For the minus DJP, both the droplets on the top and bottom sides of the step tend to move in the positive direction of the horizontal axis, while for the plus case, the droplets move in the opposite direction.

4. Conclusion

A boundary integral method with linear elements was used to study the coarsening dynamics of two interacting nanodroplets on topographical heterogeneous substrates and the effects of different parameters on the dynamics were investigated.

The step height was the first geometrical parameter for which the effect on the dynamics was investigated. It was shown that a step height increase intensifies the disjoining pressure and results in a nonlinear increase in collapse time and a transition in the droplet migration direction. Considering another physical parameter, the initial distance of the droplets from the step, made it clear that droplets far from the step exchange mass more slowly than the ones in proximity to the step. It was shown that the lateral variation of the step disjoining pressure plays an important role in this case and modifies the linear behavior observed for a homogeneous surface to a nonlinear variation. Then the reversed configuration of droplets was considered, and it was shown that the collapse time increase due to the step height increase was similar to the previous case, but there was no sign of any transition as formerly occurred in the droplet migration.

The influence of the slip boundary condition was examined by considering the slip length in a range from zero (no slip) to larger values. Consistent with the results of the coarsening on homogeneous and chemical substrates, the slip enhances the dynamics and boosts the speed of droplet migration, but a transition occurs in the droplets migration direction when the no-slip condition is changed to the slip regime.

Decreasing the surface wettability accelerates the dynamics and weakens the influence of the DJP force on the droplet migration. The last investigated parameter was the form of the disjoining pressure, and it was shown that for both types of the DJP (the minus and the plus cases) increasing B (one of the pair parameters of the DJP) enhances the dynamics. For the minus case the drops move in the positive direction of the horizontal axis, while the movement is in the opposite direction for the plus case. An approximate

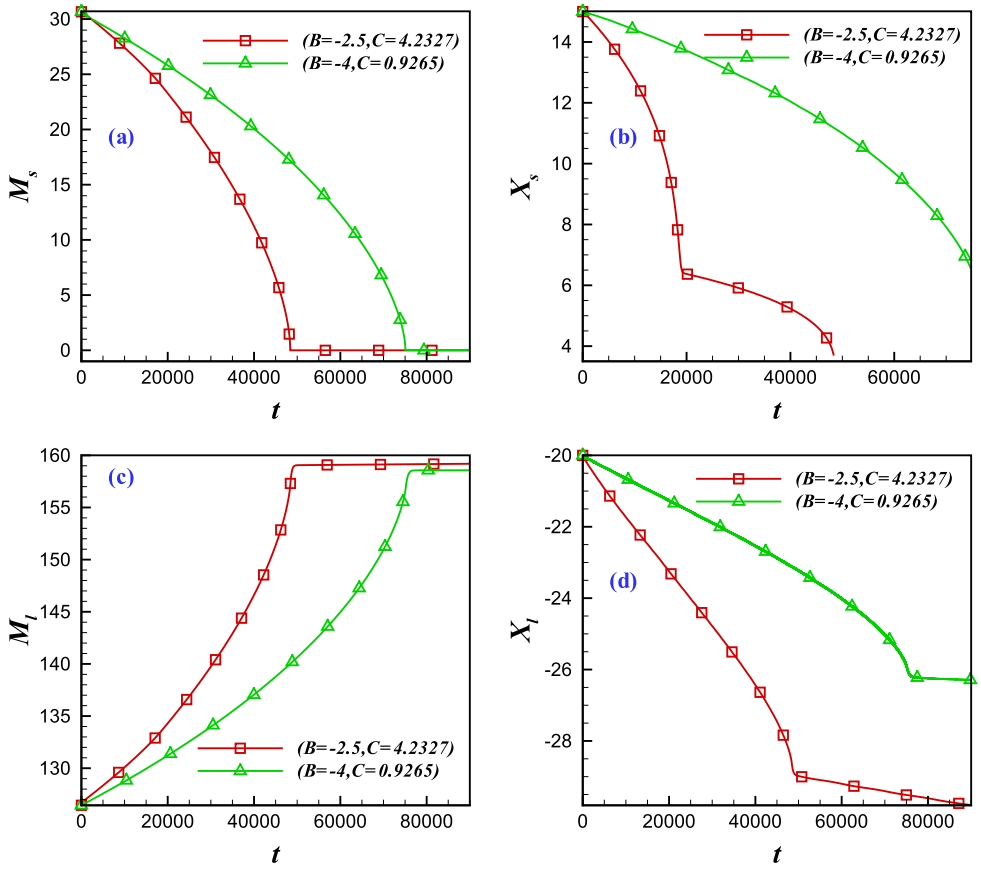

Figure 16. The effect of (B, C) of the plus disjoining pressure on the coarsening dynamics. The equilibrium contact angle is fixed for all the cases $\theta_{eq} = 90°$. The radius and height of the larger droplet are twice those of the smaller one, with values of 10 and 5, respectively. The step height is 5 and both the droplets are positioned at a distance 10 from the step $(L_1, L_2 = 10)$.

model of the DJP for the step topography was also considered and the results were compared with those of the more accurate model. The mass evolution of the droplets is almost the same for both of the models, but a huge difference is observable in the droplet migration.

To have an approximation of the time scale, we consider that the time is scaled by $\mu b/(\tilde{C}\sigma)$. Taking typical values of b and σ as 1 nm and 0.01 N m^{-1}, respectively, and considering $\tilde{C} = 3$ and $t^* \approx 30\,000$, the time can be obtained as a function of the viscosity $t = 10^{-3}\mu$. Then, considering μ between 0.1 Pa s and 100 Pa s, the time ranges from 100 μs to 0.1 s.

References

[1] Mitlin V S 1993 Dewetting of solid surface: analogy with spinodal decomposition *J. Colloid Interface Sci.* **156** 491–7

[2] Mitlin V S and Petviashvili N V 1994 Nonlinear dynamics of dewetting: kinetically stable structures *Phys. Lett.* A **192** 323–6

[3] Xie R, Karim A, Douglas J F, Han C C and Weiss R A 1998 Spinodal dewetting of thin polymer films *Phys. Rev. Lett.* **81** 1251–4

[4] Oron A and Bankoff S G 1999 Dewetting of a heated surface by an evaporating liquid film under conjoining/disjoining pressures *J. Colloid Interface Sci.* **218** 152–66

[5] Konnur R, Kargupta K and Sharma A 2000 Instability and morphology of thin liquid films on chemically heterogeneous substrates *Phys. Rev. Lett.* **84** 931–4

[6] Kargupta K and Sharma A 2002 Dewetting of thin films on periodic physically and chemically patterned surfaces *Langmuir* **18** 1893–903

[7] Kargupta K and Sharma A 2002 Creation of ordered patterns by dewetting of thin films on homogeneous and heterogeneous substrates *J. Colloid Interface Sci.* **245** 99–115

[8] Volodin P and Kondyurin A 2008 Dewetting of thin polymer film on rough substrate: II. Experiment *J. Phys. D: Appl. Phys.* **41** 065307

[9] Reiter G 1992 Dewetting of thin polymer films *Phys. Rev. Lett.* **68** 75–8

[10] Sharma A and Khanna R 1999 Pattern formation in unstable thin liquid films under the influence of antagonistic short- and long-range forces *J. Chem. Phys.* **110** 4929–36

[11] Sharma A and Khanna R 1998 Pattern formation in unstable thin liquid films *Phys. Rev. Lett.* **81** 3463–6

[12] Neto C, Jacobs K, Seemann R, Blossey R, Becker J and Grün G 2003 Satellite hole formation during dewetting: experiment and simulation *J. Phys.: Condens. Matter* **15** 3355

[13] Reiter G, Sharma A, Casoli A, David M O, Khanna R and Auroy P 1999 Thin film instability induced by long-range forces *Langmuir* **15** 2551–8

[14] Herminghaus S, Jacobs K, Mecke K, Bischof J, Fery A, Ibn-Elhaj M and Schlagowski S 1998 Spinodal dewetting in liquid crystal and liquid metal films *Science* **282** 916–9

[15] Vandenbrouck F, Valignat M P and Cazabat A M 1999 Thin nematic films: metastability and spinodal dewetting *Phys. Rev. Lett.* **82** 2693–6

[16] Valignat M P, Villette S, Li J, Barberi R, Bartolino R, Dubois-Violette E and Cazabat A M 1996 Wetting and anchoring of a nematic liquid crystal on a rough surface *Phys. Rev. Lett.* **77** 1994–7
[17] Bischof J, Scherer D, Herminghaus S and Leiderer P 1996 Dewetting modes of thin metallic films: nucleation of holes and spinodal dewetting *Phys. Rev. Lett.* **77** 1536–9
[18] Brochard-Wyart F and Redon C 1992 Dynamics of liquid rim instabilities *Langmuir* **8** 2324–9
[19] Segalman R A and Green P F 1999 Dynamics of rims and the onset of spinodal dewetting at liquid/liquid interfaces *Macromolecules* **32** 801–7
[20] Sharma A and Reiter G 1996 Instability of thin polymer films on coated substrates: rupture, dewetting, and drop formation *J. Colloid Interface Sci.* **178** 383–99
[21] Cahn J W and Hilliard J E 1958 Free energy of a nonuniform system. I. Interfacial free energy *J. Chem. Phys.* **28** 258–67
[22] Pego R L 1989 Front migration in the nonlinear Cahn–Hilliard equation *Proc. R. Soc.* A **422** 261–78
[23] Bray A J 1994 Theory of phase ordering kinetics *Adv. Phys.* **43** 357
[24] Glasner K B and Witelski T P 2003 Coarsening dynamics of dewetting films *Phys. Rev.* E **67** 016302
[25] Kitavtsev G and Wagner B 2010 Coarsening dynamics of slipping droplets *J. Eng. Math.* **66** 271–92
[26] Gratton M B and Witelski T P 2008 Coarsening of unstable thin films subject to gravity *Phys. Rev.* E **77** 016301
[27] Limary R and Green P F 2002 Late-stage coarsening of an unstable structured liquid film *Phys. Rev.* E **66** 021601
[28] Limary R and Green P F 2003 Dynamics of droplets on the surface of a structured fluid film: late-stage coarsening *Langmuir* **19** 2419–24
[29] Otto F, Rump T and Slepcev D 2006 Coarsening rates for a droplet model: rigorous upper bounds *SIAM J. Math. Anal.* **38** 503–29
[30] Kargupta K, Konnur R and Sharma A 2000 Instability and pattern formation in thin liquid films on chemically heterogeneous substrates *Langmuir* **16** 10243–53
[31] Kargupta K and Sharma A 2003 Mesopatterning of thin liquid films by templating on chemically patterned complex substrates *Langmuir* **19** 5153–63
[32] Kargupta K and Sharma A 2002 Morphological self-organization by dewetting in thin films on chemically patterned substrates *J. Chem. Phys.* **116** 3042
[33] Kargupta K and Sharma A 2001 Templating of thin films induced by dewetting on patterned surfaces *Phys. Rev. Lett.* **86** 4536–9
[34] Sharma A, Konnur R and Kargupta K 2003 Thin liquid films on chemically heterogeneous substrates: self-organization, dynamics and patterns in systems displaying a secondary minimum *Physica* A **318** 262–78
[35] Kao J C T, Golovin A A and Davis S H 2006 Rupture of thin films with resonant substrate patterning *J. Colloid Interface Sci.* **303** 532–45
[36] Thiele U, Brusch L, Bestehorn M and Bär M 2003 Modelling thin-film dewetting on structured substrates and templates: bifurcation analysis and numerical simulations *Eur. Phys. J.* E **11** 255–71
[37] Ondarçuhu T and Piednoir A 2005 Pinning of a contact line on nanometric steps during the dewetting of a terraced substrate *Nano Lett.* **5** 1744–50
[38] Simmons D and Chauhan A 2006 Influence of physical and chemical heterogeneity shape on thin film rupture *J. Colloid Interface Sci.* **295** 472–81
[39] Ajaev V S, Gatapova E Y and Kabov O A 2011 Rupture of thin liquid films on structured surfaces *Phys. Rev.* E **84** 041606
[40] Cavallini M, Gomez-Segura J, Albonetti C, Ruiz-Molina D, Veciana J and Biscarini F 2006 Ordered patterning of nanometric rings of single molecule magnets on polymers by lithographic control of demixing *J. Phys. Chem.* B **110** 11607–10
[41] Asgari M and Moosavi A 2012 Coarsening dynamics of dewetting nanodroplets on chemically patterned substrates *Phys. Rev.* E **86** 016303
[42] Moosavi A, Rauscher M and Dietrich S 2009 Dynamics of nanodroplets on topographically structured substrates *J. Phys.: Condens. Matter* **21** 464120
[43] Kelmanson M A 1983 Boundary integral equation solution of viscous flows with free surfaces *J. Eng. Math.* **17** 329–43
[44] Brusch L, Kühne H, Thiele U and Bär M 2002 Dewetting of thin films on heterogeneous substrates: pinning versus coarsening *Phys. Rev.* E **66** 011602
[45] Bielarz C and Kalliadasis S 2003 Time-dependent free-surface thin film flows over topography *Phys. Fluids* **15** 2512
[46] Gaskell P H, Jimack P K, Sellier M and Thompson H M 2004 Efficient and accurate time adaptive multigrid simulations of droplet spreading *Int. J. Numer. Methods Fluids* **45** 1161–86
[47] Yochelis A, Knobloch E and Pismen L M 2007 Formation and mobility of droplets on composite layered substrates *Eur. Phys. J.* E **22** 41–9
[48] Moosavi A, Rauscher M and Dietrich S 2006 Motion of nanodroplets near edges and wedges *Phys. Rev. Lett.* **97** 236101
[49] Glasner K B, Otto F, Rump T and Slepcev D 2009 Ostwald ripening of droplets: the role of migration *Eur. J. Appl. Math.* **20** 1–67
[50] de Gennes P G, Brochard-Wyart F and Quere D 2003 *Capillarity and Wetting Phenomena: Drops, Bubbles, Pearls, Waves* (Berlin: Springer)